Nuclear Engineering and Technology 48 (2016) 1291–1302

Available online at ScienceDirect

Nuclear Engineering and Technology

journal homepage: www.elsevier.com/locate/net

Original Article

A Study on the Optimal Position for the Secondary Neutron Source in Pressurized Water Reactors

Jungwon Sun [a], *Mohd-Syukri Yahya* [b], *and Yonghee Kim* [b,*]

[a] *KEPCO Nuclear Fuel, 242 Daedeok-daero 989beon-gil, Yuseong-gu, Daejeon 34057, Republic of Korea*
[b] *Department of Nuclear and Quantum Engineering, Korea Advanced Institute of Science and Technology (KAIST), 291 Daehak-ro, Yuseong-gu, Daejeon, 34141, Republic of Korea*

ARTICLE INFO

Article history:
Received 23 December 2015
Received in revised form
4 May 2016
Accepted 8 May 2016
Available online 25 May 2016

Keywords:
Adjoint Flux
Boron Dilution Accident
ICRR Curve
Monte Carlo Analysis
Neutron Source
PWR

ABSTRACT

This paper presents a new and efficient scheme to determine the optimal neutron source position in a model near-equilibrium pressurized water reactor, which is based on the OPR1000 Hanul Unit 3 Cycle 7 configuration. The proposed scheme particularly assigns importance of source positions according to the local adjoint flux distribution. In this research, detailed pin-by-pin reactor adjoint fluxes are determined by using the Monte Carlo KENO-VI code from solutions of the reactor homogeneous critical adjoint transport equations. The adjoint fluxes at each allowable source position are subsequently ranked to yield four candidate positions with the four highest adjoint fluxes. The study next simulates ex-core detector responses using the Monte Carlo MAVRIC code by assuming a neutron source is installed in one of the four candidate positions. The calculation is repeated for all positions. These detector responses are later converted into an inverse count rate ratio curve for each candidate source position. The study confirms that the optimal source position is the one with very high adjoint fluxes and detector responses, which is interestingly the original source position in the OPR1000 core, as it yields an inverse count rate ratio curve closest to the traditional 1/M line. The current work also clearly demonstrates that the proposed adjoint flux-based approach can be used to efficiently determine the optimal geometry for a neutron source and a detector in a modern pressurized water reactor core.

1. Introduction

Excore neutron detectors are used to monitor reactivity states of commercial pressurized water reactors (PWRs) with the aid of the inverse count rate ratio (ICRR) curve. In the ICRR curve, the normalized ratio of the source range detector count rates to the reference signals is calculated and extrapolated to zero at criticality. The detector signals must exceed a specified

* *Corresponding author.*
E-mail address: yongheekim@kaist.ac.kr (Y. Kim).
http://dx.doi.org/10.1016/j.net.2016.05.002

minimum count rate, which necessitates the use of secondary neutron sources to ensure neutron levels are high enough to be detected by nuclear instruments at all times, especially during subcritical startup operation of the PWR. For example, californium-252 (^{252}Cf) is used to supply source neutrons in initial cores while antimony–beryllium (Sb-Be) is used in reload cores. In near-equilibrium cycles, however, neutrons from spontaneous fissions of actinides such as those of curium-242 (^{242}Cm) and curium-244 (^{244}Cm) are sufficiently high to yield the minimum detector count rates. In this regard, secondary neutron sources are unnecessary and, therefore, removed from the near-equilibrium PWR cores. Removal of these highly radioactive non-nuclear materials is also advantageous since it reduces the risk of accidental coolant activation from any probable breach in the neutron source assemblies [1]. Secondary neutron sources are, in fact, only used up to Cycle 5 or 6 in standard Korean OPR1000 core designs [2].

However, one must note that modern PWR cores normally load highly-burned fuel assemblies on their periphery in pursuit of high neutron economy. In a highly subcritical near-equilibrium core, such as during all-rod-in (ARI) startup operation, this low-leakage core in tandem with the absence of secondary neutron sources significantly suppresses the ex-core detector count rates and, therefore, severely limits the detector sensitivity. As a result, reactivity monitoring with the ICRR curve can be misleading [3–5]. This is because the measured ICRR curve in the core can actually be highly nonlinear while the theoretical ICRR curve used in the core reactivity warning system, such as the boron dilution alarm setpoint (BDAS), is linear. The discrepancy between the actual nonlinear ICRR curve and the ideal ICRR curve is illustrated in Fig. 1 [3]. This possibly results in a noticeable time delay in the boron dilution alarm system, which adversely affects the core reactivity monitoring and compromises the overall reactor safety. This safety concern is highlighted in the United States Nuclear Regulatory Commission's information notice 93-32 that warns of the possible loss of shutdown margin at the Comanche Peak Steam Electric Station due to its nonconservative BDAS determination [6]. In particular, the predetermined BDAS, which is based on the traditional subcritical multiplication theory, may only be triggered after an appreciable amount of boron dilution has occurred in the core. This unmitigated boron dilution event is regarded by the United States Nuclear Regulatory Commission as a serious breakdown which requires adequate protection action [7]. Similar concern over the nonconservative ICRR curve behavior was also observed during a postulated boron dilution event at shutdown with all rods inserted at the Diablo Canyon nuclear power station [3].

One possible solution is to install secondary neutron sources in the near-equilibrium PWR cores so as to "make" its ICRR curve linear again. Note that the efficiency and functionality of the secondary neutron source depends greatly on its location in the core. As such, an optimal position exists where the source efficiency is optimized in terms of the neutron source importance, ex-core detector responses, and linearity of the corresponding ICRR curve.

The simplest method to determine such an optimal source position is by performing a direct exhaustive search, i.e., evaluating detector responses for each allowable neutron source location separately. This is, however, very time consuming. Moreover, all of the calculations must be painstakingly repeated should there be any design change in the ex-core detector system. A more efficient methodology is thereby needed.

This paper proposes a unique adjoint flux-based approach to efficiently determine the optimal source-detector geometry in a modern PWR core. In this research, the source position is evaluated by taking into account its contribution to the fission reaction in the core instead of evaluating the conventional neutron importance to the ex-core detector signal. As such,

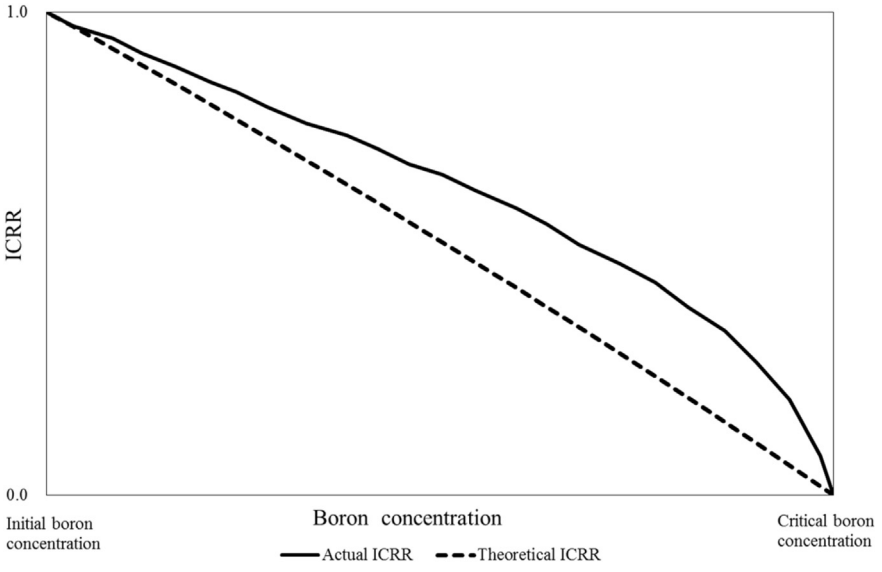

Fig. 1 – Illustrative discrepancy between the actual inverse count rate ratio (ICRR) curve and the theoretical 1/M line against boron concentration in the core.

the importance of the secondary source position can be determined by solving the reactor adjoint equation just once, regardless of the ex-core detector position and designs. It should be noted that this approach is based on the general assumption that the more fission neutrons produced by the secondary source, the higher the detector signal would be. On the other hand, the source importance to an ex-core detector in the conventional approach should be re-evaluated if the ex-core detector position or design is changed. This paper is organized as follows: Section 2 presents the fundamental concepts of homogeneous reactor adjoint equations, Section 3 describes the calculations performed using the Monte Carlo KENO-VI [8,9] and Monte Carlo MAVRIC [10] codes, Section 4 discusses simulation results, and Section 5 presents conclusions of the work.

2. Basic theories and concepts

Subcritical neutron multiplication is an estimate of how far the reactor is from criticality. It is related to the total number of neutrons produced by a single neutron source as follows [11]:

$$\begin{aligned} N_{total}^{sub} &= \{[(S\cdot k_{eff}+S)\cdot k_{eff}+S]\cdot k_{eff}+S\ldots\} \\ &= S\cdot\left(1+k_{eff}+k_{eff}^2+k_{eff}^3+\ldots\right) \\ \frac{1}{1-k_{eff}}\cdot S &= M\cdot S \end{aligned} \tag{1}$$

where S is external source strength, k_{eff} is effective neutron multiplication factor, and M is the subcritical multiplication factor which represents the fractional change in the neutron population of a subcritical reactor due to changes in the core reactivity. Note that Eq. (1) does not provide the time required for criticality. In fact, as k_{eff} approaches 1.0, it takes more time for the neutron levels to stabilize. This, thus, explains the characteristically slow and steady startup operation of a commercial PWR so as to accommodate sufficient time for the reactor to attain equilibrium. Since the equilibrium neutron level in a subcritical reactor is proportional to the initial neutron source strength, it is important to set a minimum neutron count rate during the startup operation.

The detector count rate in a subcritical reactor by itself is not a perfect representation of neutron activity in the core. Count rate ratios are instead more useful to monitor a reactor's response to reactivity changes and approach to criticality. In the subcritical reactivity monitoring with the ICRR curve, the inverse of the subcritical multiplication factor (1/M) is normalized such that when the core approaches criticality (1.0), 1/M edges to 0 in a negative linear correlation as shown in Fig. 2. However, the ICRR curve can actually be nonlinear when there is no secondary neutron source or the ex-core detector sensitivity is very low.

Meanwhile, the time-independent neutron transport equation of a nuclear reactor without an external neutron source is:

$$A\Phi_{critical} = \frac{1}{k_{eff}}F\Phi_{critical} \tag{2}$$

where A is the net neutron loss (i.e., leakage + absorption) operator, F is the fission production operator, and $\Phi_{critical}$ is forward neutron flux in the critical reactor. Similarly, the neutron transport equation in a stationary subcritical system with an external source $S(r, E, \Omega)$ is:

$$A\Phi_{subcritical} = F\Phi_{subcritical} + S \tag{3}$$

where $\Phi_{subcritical}$ is forward neutron flux in the subcritical reactor. The inhomogeneous solution of Eq. (3) represents the neutron flux distribution (or source multiplication) of the core, which strongly depends on the neutron source's position (r), energy (E), and emission direction (Ω).

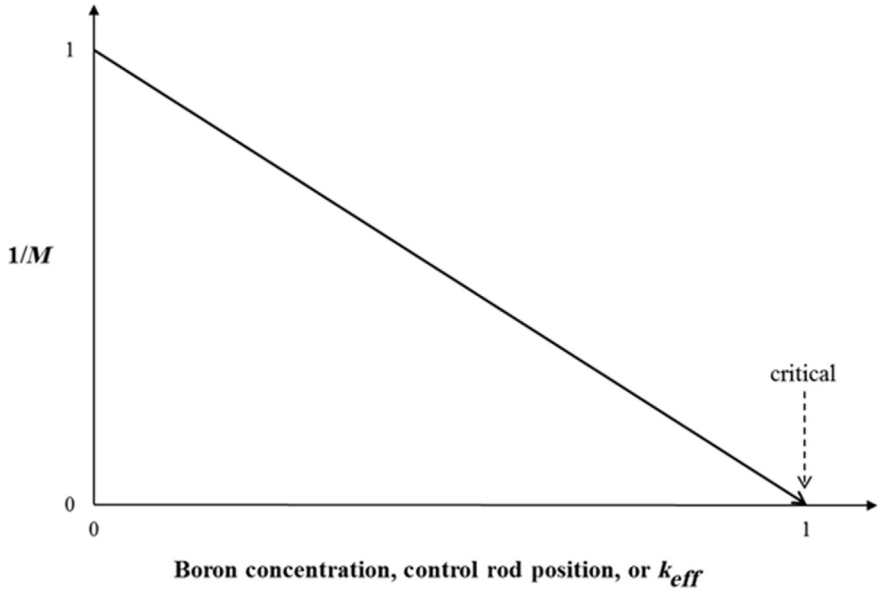

Fig. 2 – Normalized 1/M versus boron concentration, control rod position, or k_{eff}.

Table 1 – Design parameters of the H3C7 core [2].

Parameter	Value
No. of fuel assemblies	177
No. of control element assemblies	73
No. of fuel rods	41,772
No. of shim rods	768
Fuel assembly lattice array	16 × 16
Fuel rod pitch (cm)	1.285
Outside fuel assembly dimension (cm)	20.25

Source multiplication factor k_{src}, which is the ratio of neutron production to loss in a subcritical reactor with an external source, can therefore be approximated from Eqs. (2) and (3) as follows [12]:

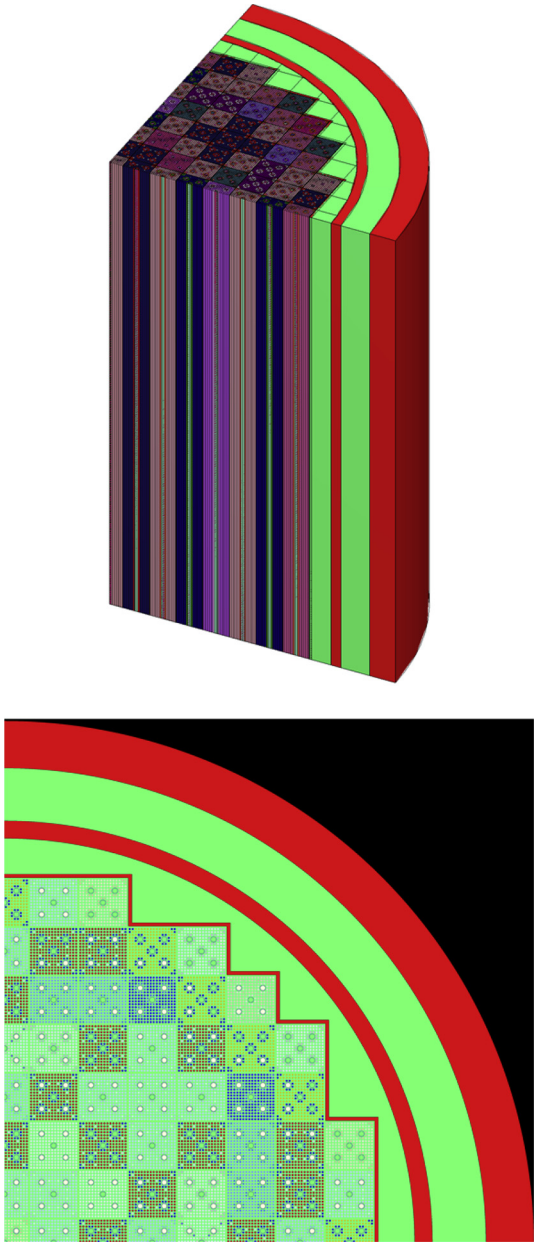

Fig. 3 – Three-dimensional quarter-core KENO-VI model of the Hanul Unit 3 Cycle 7 core.

Table 2 – Major isotopes tracked in the fuel compositions [18].

U-234	U-235	U-236	U-238	Np-237
Pu-238	Pu-239	Pu-240	Pu-241	Pu-242
Am-241	Am-242*	Am-243	Cm-242	Cm-243
Cm-244	Kr-83	Kr-85	Sr-90	Y-89
Mo-95	Zr-93	Zr-94	Zr-95	Tc-99
Ru-101	Ru-106	Rh-103	Rh-105	Pd-105
Pd-108	Ag-109	Sb-124	Xe-131	Xe-132
Xe-135	Xe-136	Cs-133	Cs-134	Cs-135
Cs-137	Ba-136	La-139	Ce-144	Pr-141
Pr-143	Nd-143	Nd-145	Nd-147	Pm-147
Pm-148	Sm-147	Sm-149	Sm-150	Sm-151
Sm-152	Eu-153	Eu-154	Eu-155	Gd-155

$$k_{src} = \frac{\text{neutron production rate}}{\text{neutron loss rate}} = \frac{\langle F\Phi_{subcritical}\rangle}{\langle A\Phi_{subcritical}\rangle} = \frac{\langle F\Phi_{subcritical}\rangle}{\langle F\Phi_{subcritical}\rangle + \langle S\rangle} \tag{4}$$

where brackets imply integration over space, angle, and energy domains. One notes that k_{scr} is essentially the ratio of fission to total neutrons produced (both fission and external sources).

Neutron source efficiency φ^*, an index indicating its importance relative to the fission, can thereby be defined as:

$$\varphi^* = \frac{\left(\frac{1-k_{eff}}{k_{eff}}\right)}{\left(\frac{1-k_{src}}{k_{src}}\right)} \tag{5}$$

which, via substitution of Eq. (4) into Eq. (5), simply becomes:

$$\varphi^* = \left(\frac{1-k_{eff}}{k_{eff}}\right)\cdot\frac{\langle F\Phi_{subcritical}\rangle}{\langle S\rangle} \tag{6}$$

In essence, the source efficiency implies how much the neutron source contributes to the final fission events and total power of the system. One must also note that φ^* strongly depends on the source's position, energy, and emission direction. For example, a neutron source with a high fission probability will have a high importance, as will a source with a low leakage probability. In addition, the source neutron in a

Table 3 – Design parameters of the secondary Sb-Be neutron source [2].

Component	Value
Pellet	
Material	Sb-Be
Diameter (cm)	1.66
Density (g/cm^3)	
Antimony 124 (^{124}Sb)	6.68
Beryllium 9 (^{9}Be)	1.85
Tube	
Material	SS-316
Length (cm)	101.96
Outside diameter (cm)	2.0625
Inside diameter (cm)	1.6767
Density (g/cm^3)	7.75

subcritical reactor can be made more important by positioning it in a highly reactive fuel region. Therefore, for a given source importance, the subcritical multiplication factor M can be improved by multiplying it with the neutron source efficiency as follows:

$$M_i = \frac{1}{1-k_{eff}}\varphi^* = M\varphi^* \quad (7)$$

where M_i is the *improved* source multiplication factor.

Eq. (7) clearly requires the source importance to be near unity for the improved ICRR curve to be linear. As such, fission neutron multiplication due to the secondary source should be as large as technically possible. In other words, the position of the secondary source should be optimized so as to maximize its importance for the fission, which can be determined by solving the reactor adjoint neutron transport equations [13–16].

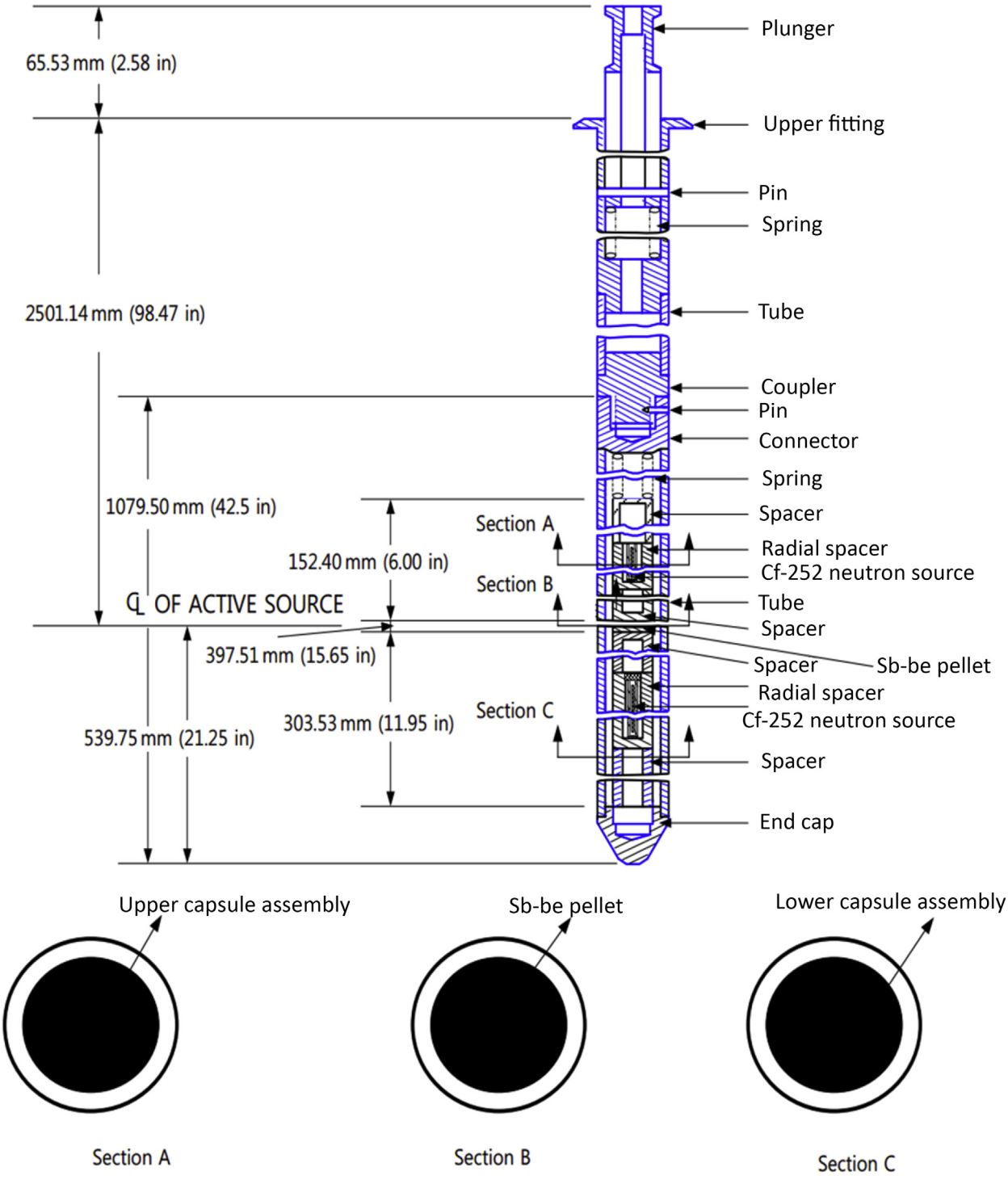

Fig. 4 – Neutron source assembly for the OPR1000 core.

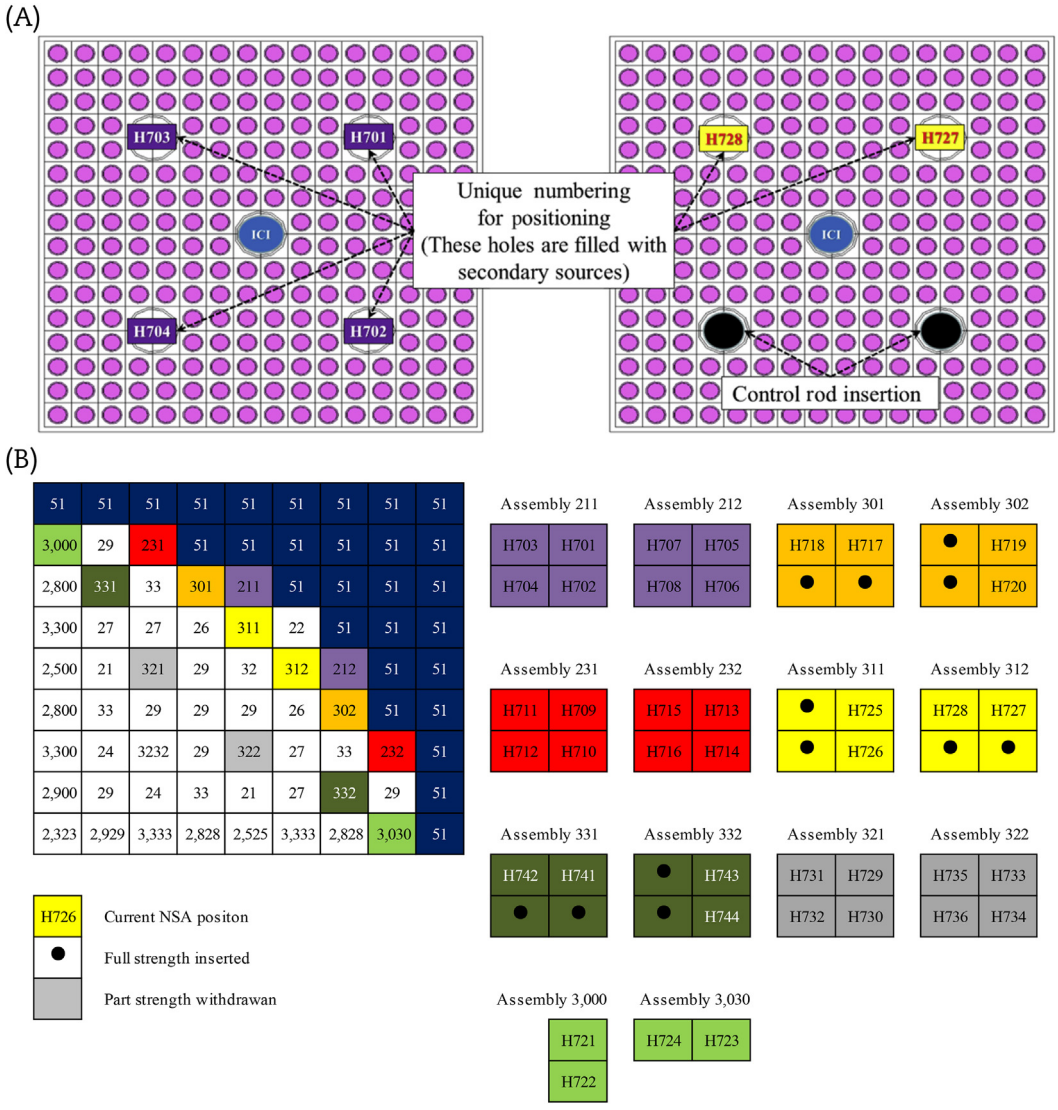

Fig. 5 – Sequential numbering system for the candidate source positions. (A) Representative H3C7 fuel assembly with five guide tubes. (B) Radial view of the core source installation. NSA, neutron source assembly.

In a subcritical system with a fixed secondary source, the adjoint problem can be approximated as follows:

$$A^{\dagger}\Phi^{\dagger}_{subcritical} = F^{\dagger}\Phi^{\dagger}_{subcritical} + S^{\dagger} \tag{8}$$

where $A^{\dagger}$ is the adjoint operator for net neutron loss (i.e., leakage + absorption), $F^{\dagger}$ is the adjoint operator for fission production, and $S^{\dagger}$ is the adjoint external source. In this work, the source neutron importance is defined in terms of its contribution to the fission reaction in the subcritical reactor. In order to determine the source neutron importance, the adjoint external source is thereby set as $S^{\dagger} = -\upsilon\Sigma_f$.

Meanwhile, adjoint flux in a homogeneous reactor can be determined from the following conventional homogeneous adjoint reactor equation [15]:

$$A^{\dagger}\Phi^{\dagger}_{critical} = \frac{1}{k_{eff}}F^{\dagger}\Phi^{\dagger}_{critical} \tag{9}$$

where $\Phi^{\dagger}_{critical}$ is the adjoint flux in a critical reactor. One notes that Eq. (9) represents fission neutron importance in terms of its contribution to the fission reaction rate in a critical reactor. In other words, the importance of a fission neutron is proportional to the number of fission neutrons generated by the neutron.

There is a clear similarity between $\Phi^{\dagger}_{subcritical}$ in Eq. (8) and $\Phi^{\dagger}_{critical}$ in Eq. (9) [15], which implies that neutron source importance in a subcritical core can indirectly be determined by calculating the adjoint flux in its corresponding homogeneous critical reactor. This is another unique feature of our proposed approach. Rather than determining the exact source importance in view of its contribution to the fission reaction in the subcritical reactor by solving Eq. (8), which mathematically depends on the source itself, this research proposes solving the conventional homogenous adjoint equation in Eq. (9) instead. In this approach, the importance needs to be evaluated only once

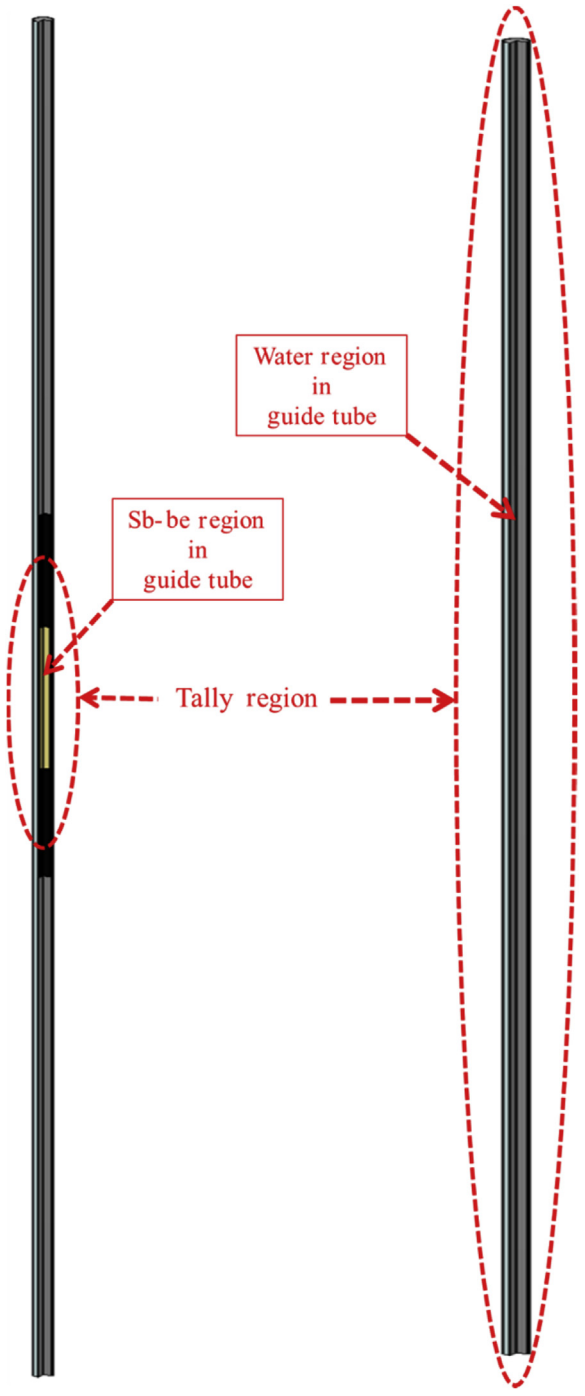

Fig. 6 – Adjoint flux tally regions for the two KENO-VI simulations.

regardless of the source itself. The validity of this approach was largely documented in Kim et al. [15], in which the external source importance for an accelerator-driven subcritical system was evaluated with the aforementioned approach and it was clearly demonstrated that the simple homogeneous adjoint fluxes are very similar to the actual source neutron importance obtained by solving Eq. (8).

In addition to having a very high neutron source importance, the secondary neutron source should also yield reasonably high detector responses, so as to assure a fairly high source range detector sensitivity. The location of the secondary source in the PWR core majorly governs these two desired characteristics (i.e., high neutron source importance and high detector sensitivity). From past experiences, it is clear that the secondary neutron source should be installed far from control rods, nearby reactive fuel assemblies, and on the sub-inner core ring. In this research, neutron source importance in terms of the fission contribution in the modeled subcritical reactor was uniquely determined by solving Eq. (9) using the Monte Carlo KENO-VI code with the 238-group SCALE nuclear data library [17]. Meanwhile, the corresponding source range detector responses were calculated from solutions of the reactor forward equation by postulating a boron dilution accident (BDA) using the Monte Carlo MAVRIC code.

3. The model Hanul Unit 3 Cycle 7 reactor

3.1. *Homogeneous adjoint flux calculations using Monte Carlo KENO-VI code*

The Monte Carlo KENO-VI code, which was developed by Oak Ridge National Laboratory, Oak Ridge, TN, USA can be used to calculate multiplication factors, forward and adjoint flux distributions, fission densities, and other physics parameters of a fissile system. Note that adjoint calculations with the KENO-VI code are relatively simple due to the multi-group cross-section treatment in the code. This is because the entire cross-section processing sequences are automatically performed in adjoint mode prior to exporting the transposed scattering matrix to the KENO-VI solver. The code then automatically calculates all energy-related adjoint quantities such as cross-section group structures, weighting and albedo data, fission spectra, etc. The calculated energy-dependent adjoint fluxes, in units of neutrons/cm^2/source neutron, thus represent the relative contribution of a neutron, at a specific energy and position, to the total fissions in the system.

The PWR design modeled in this work is based on the Hanul Unit 3 Cycle 7 (H3C7) reactor [2]. Major design parameters of the core are listed in Table 1. The three-dimensional quarter-core was modeled in full to include baffle, barrel and vessel, and concrete wall components, as shown in Fig. 3. The adjoint flux calculations were performed at cold zero power conditions with moderator temperature set at 20°C, ARI in which all control and shutdown rods are fully inserted, and with boron concentration of 2,223 ppm. It was also assumed that all part-strength control rods are fully withdrawn from the core. All 60 major isotopes tracked in the fuel compositions are tabulated in Table 2 [18].

Two KENO-VI simulations were performed in this study: the first on the H3C7 core with Sb-Be secondary neutron sources and the second without any source, representing two "extremes" of the simulated scenarios. In the first simulation (with neutron source), the secondary neutron sources are

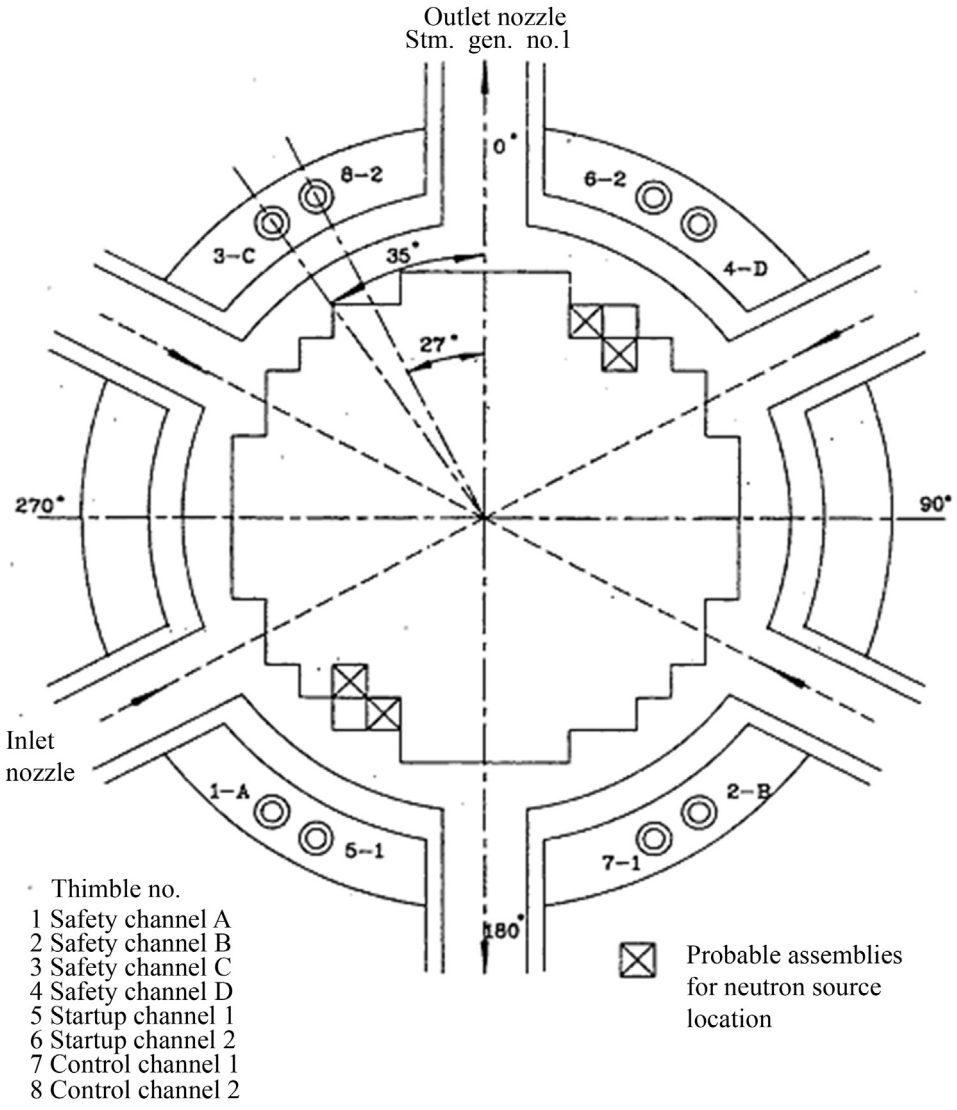

Fig. 7 – Radial view of the ex-core detector channels in H3C7, Hanul Unit 3 Cycle 7 core [2]. Stm. gen., steam generator.

inserted in all empty nonrodded guide tubes. Details of the secondary Sb-Be neutron source assemblies modeled are available in Table 3 and Fig. 4. In the second simulation (without neutron source), the empty nonrodded guide tubes are filled with water. Each of the empty guide tubes in the two simulations, including those loaded with part-strength control rods, is labeled with a unique numbering sequence as depicted in Fig. 5. Note that the central guide tube in Fig. 5A is reserved for the fixed in-core detector while the white-colored boxes in Fig. 5B are rodded fuel assemblies and, therefore, excluded from the adjoint flux calculations. Fig. 6 depicts tally regions of the adjoint flux calculations: adjoint flux is tallied in the Sb-Be source region only in the first simulation, while the flux tally region envelops the whole length of the guide tube in the second simulation.

3.2. *Ex-core detector response calculations using Monte Carlo MAVRIC code*

Fig. 7 depicts the radial view of eight ex-core detector channels in the H3C7 core. Each of the ex-core detector channels is loaded with three detectors in symmetry with respect to the core mid-plane. The detector is based on a boron-10 (^{10}B) proportional counter with macroscopic cross-section about 2.714729×10^{-5}/cm. In this study, the ex-core detector signals for a given secondary source were calculated using the Monte Carlo MAVRIC code from solutions of the reactor forward equations. Since standard Sb-Be neutron sources installed in typical OPR1000 cores produce source neutrons of ~23-keV energy, the simulated photo-neutron Sb-Be source was thereby assumed to emit isotopic and mono-energetic 10^8

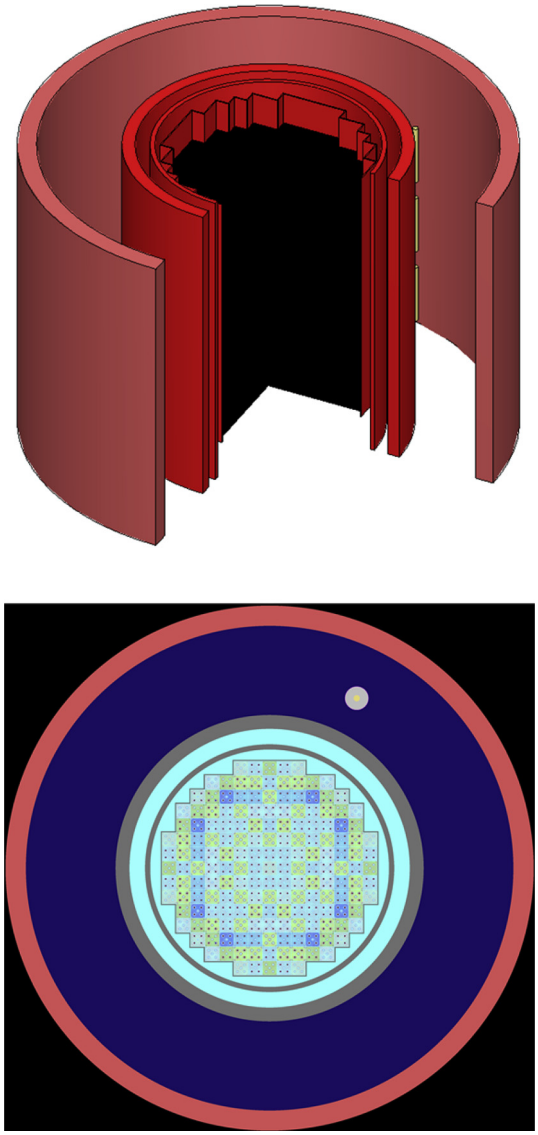

Fig. 8 – Full three-dimensional Hanul Unit 3 Cycle 7 core geometry modeled with the MAVRIC reactor.

neutrons/s with 23-keV energy each. Detector responses or reaction rates are estimated based on the MAVRIC forward solutions using American National Standards Institute standard neutron and gamma-ray flux-to-dose conversion factors.

Table 4 – Summary of KENO-VI simulation results.

Parameter	H3C7 with neutron source	H3C7 without neutron source
Best estimate k_{eff}	0.873742 ± 0.000047	0.874500 ± 0.00019
Energy of average fission lethargy (eV)	0.0014 ± 4.9772E-08	0.0014 ± 1. 9837E-07
System nu bar k_{eff}	1.4616 ± 6.8264E-05	1.4629 ± 2.7140E-04
System mean free path (cm)	0.7351 ± 4.9203E-06	0.7343 ± 1.8923E-05
Computing time (min)	63,692	4,387

H3C7, Hanul Unit 3 Cycle 7.

Note that the ICRR curve for a given secondary source can be calculated from a series of MAVRIC detector response calculations at different core reactivity conditions. For example, the ICRR curve during a BDA can be determined by performing the MAVRIC analyses for a set of different boron concentrations in the coolant.

The three-dimensional H3C7 reactor with one ex-core detector was modeled in full (not quarter-core) as depicted in Fig. 8 so as to simulate the neutron leakage more accurately. Note that only one out of eight possible ex-core detector channels was modeled in this study to simplify the computing-intensive simulations. This is nonetheless acceptable because the responses of all detector channels can be assumed to be identical.

4. Results and analysis

Table 4 summarizes the KENO-VI simulation results, while Table 5 lists all calculated adjoint fluxes at 23 keV in descending order. In the first KENO-VI simulation (with neutron source), the highest adjoint flux occurs at position H733 while in the second simulation (without a neutron source), the highest adjoint flux is found at position H728. Adjoint fluxes in the first simulation are generally bigger than in the second simulation due to the presence of secondary neutron sources.

Table 6 lists four candidate source positions, which are shortlisted from the top three rows of Table 5, for the subsequent MAVRIC detector response calculations. Fig. 9 depicts the locations of the four candidate source positions in the H3C7 core. Positions H733 and H729 are in symmetry on the inner core region, while positions H726 and H728 are also in symmetry but on the core subperiphery. Note that the modeled ex-core detector is much closer to positions H729 and H726 than to their counterparts.

Table 7 tabulates results of the subsequent MAVRIC simulations. It is clear that position H733, where the highest adjoint fluxes were found in the first KENO-VI simulation, consistently yields the lowest ex-core detector responses. This is expected because it is actually the farthest from the detector; i.e., signals from position H733 have to travel the longest to reach the ex-core detector, effectively increasing its attenuation cross section. Conversely, source positions H726 and H728 yield higher responses due to their closer proximity to the detector. Nonetheless, it should be noted that the detector signals are actually normalized in the ICRR curve evaluations. The ICRR curve must therefore be separately evaluated for all four candidate source positions.

In this study, a BDA during ARI core configuration was considered. The BDA was simulated by diluting boron concentrations in the coolant step-wise from 1,726 ppm to 850 ppm, at which point the reactor was assumed critical. However, Monte Carlo MAVRIC calculations are very time consuming especially when the core approaches criticality; i.e., as k_{eff} approaches 1.0, it takes longer for the neutron levels to stabilize. It was almost impossible to obtain statistically meaningful results for simulations lower than 1,288 ppm boron concentration on the current computing setup (a quad-core central processing unit with 32-GB random-access

Table 5 – Adjoint fluxes at all possible source positions for the two KENO-VI simulations.

Simulation 1: H3C7 with neutron source				Simulation 2: H3C7 without neutron source			
Ranking	Guide tube position	Adjoint flux at 23 keV (ns/cm^2/source neutron)	Statistical error (%)	Ranking	Guide tube position	Adjoint flux at 23 keV (ns/cm^2/source neutron)	Statistical error (%)
1	H733	1.6535E-08	0.5638	1	H728	8.9806E-09	0.5500
2	H728	1.5079E-08	0.5269	2	H726	8.8485E-09	0.5569
3	H729	1.1945E-08	0.5638	3	H733	8.2498E-09	0.5969
4	H731	1.1026E-08	0.6238	4	H729	7.8345E-09	0.5869
5	H708	1.0505E-08	0.7069	5	H730	6.9039E-09	0.6000
6	H735	1.0391E-08	0.5838	6	H735	6.8822E-09	0.6069
7	H726	9.4579E-09	0.5338	7	H734	6.6456E-09	0.6508
8	H719	9.2770E-09	0.6969	8	H725	6.3119E-09	0.6238
9	H734	9.1373E-09	0.6169	9	H727	6.2888E-09	0.6369
10	H707	8.9433E-09	0.8808	10	H736	6.2479E-09	0.6569
11	H725	8.8412E-09	0.6069	11	H731	6.2078E-09	0.6400
12	H704	8.3935E-09	0.7038	12	H732	5.8163E-09	0.6538
13	H730	8.3353E-09	0.5769	13	H720	5.6904E-09	0.7038
14	H718	7.3272E-09	0.6638	14	H718	5.1778E-09	0.6900
15	H727	7.2282E-09	0.6069	15	H717	5.1170E-09	0.7438
16	H744	7.1043E-09	0.9938	16	H708	5.0415E-09	0.7438
17	H732	6.9730E-09	0.6369	17	H704	4.9892E-09	0.7438
18	H741	6.1100E-09	0.8269	18	H719	4.6828E-09	0.7369
19	H720	6.0314E-09	0.6531	19	H741	3.7005E-09	0.8638
20	H702	6.0099E-09	0.8769	20	H707	3.4055E-09	0.9238
21	H736	5.5452E-09	0.6269	21	H743	3.2978E-09	0.8838
22	H717	5.2735E-09	0.7069	22	H702	2.8919E-09	0.9138
23	H743	4.3345E-09	0.8269	23	H703	2.7811E-09	0.9977
24	H706	3.7608E-09	0.9469	24	H744	2.3757E-09	1.0369
25	H742	3.5992E-09	1.0038	25	H742	2.3642E-09	1.0377
26	H715	2.9163E-09	1.1400	26	H716	2.3148E-09	1.1638
27	H716	2.8392E-09	1.0900	27	H706	2.2899E-09	0.9977
28	H703	2.0638E-09	0.9638	28	H712	1.8903E-09	1.1677
29	H710	1.9828E-09	1.1608	29	H710	1.8202E-09	1.2038
30	H705	1.9222E-09	1.3346	30	H715	1.8035E-09	1.2038
31	H712	1.7840E-09	1.1100	31	H701	1.3299E-09	1.3608
32	H701	1.4355E-09	1.3269	32	H705	1.2918E-09	1.3746
33	H711	1.2886E-09	1.7338	33	H714	8.8514E-10	1.7808
34	H714	1.1722E-09	1.7146	34	H711	8.5892E-10	1.7777
35	H724	9.5601E-10	1.7623	35	H724	7.3395E-10	1.8169
36	H722	8.9874E-10	1.7469	36	H722	7.2032E-10	1.8054
37	H713	6.8515E-10	1.9192	37	H713	6.2322E-10	2.0315
38	H709	6.3315E-10	1.9800	38	H709	5.7556E-10	2.0169
39	H721	5.6128E-10	2.3662	39	H721	4.1675E-10	2.4669
40	H723	4.5440E-10	2.4177	40	H723	4.1613E-10	2.4569

memory). As such, the ICRR curves in this study were evaluated at four dilution steps from 1,726 ppm to 1,288 ppm only.

Fig. 10 plots ICRR curves for the four candidate source positions at four boron dilution steps against a linear-fit 1/M line. Numerical values of the plotted ICRR curves are listed in Table 8. Note that although statistical uncertainties of the simulations are big and the plotted ICRR curves are incomplete (i.e., they stop short of reaching criticality), one can still derive a number of interesting observations from the analyses. Firstly, the time delay associated with the BDAS warning system is apparently eliminated by installing a secondary neutron source in the near-equilibrium PWR core. This is because the calculated ICRR curves are now under (rather than above) the theoretical 1/M curve, effectively providing a desirably longer response time to the operators in the event of a BDA. Secondly, it is clear that the optimal source position in the modeled reactor, which yields the closest ICRR curve to the conservative 1/M line, is position H726 (or alternatively, its symmetrical counterpart the H728 position). Interestingly, this is actually the designed secondary neutron source position in a typical OPR1000 core. As such, this confirms our proposed approach of choosing the optimal secondary neutron source position in the PWR core with regards to its source importance and detector response. However, one must

Table 6 – Four candidate source positions for the MAVRIC calculations.

Ranking	Source position
1	H733
2	H728
3	H729
4	H726

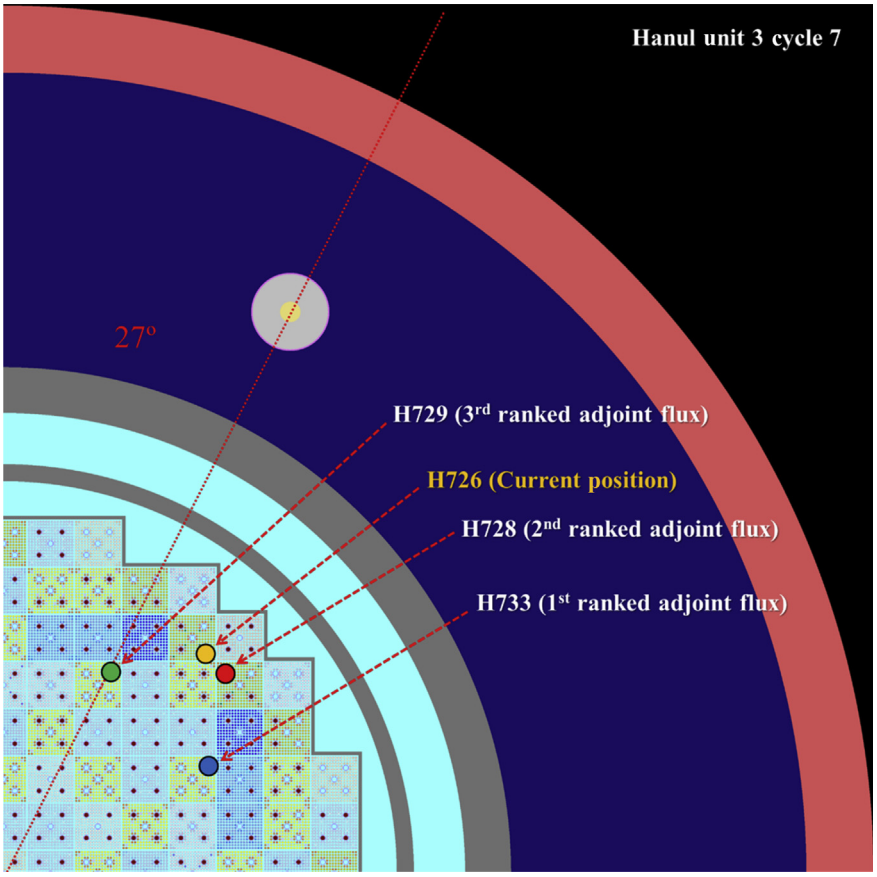

Fig. 9 – Four candidate source positions for the inverse count rate ratio evaluations.

note that the optimal secondary source position can actually be different depending on the control rod bank patterns and the effective source-detector geometry in the core.

5. Conclusion

Reactivity monitoring using the ICRR curve in a near-equilibrium subcritical PWR can be misleading. This is because while the theoretical ICRR curve used to determine the reactivity alarm set-points is linear, the measured ICRR curve in the core can actually be nonlinear. To correct this discrepancy, it has been suggested that secondary neutron sources can be installed in the near-equilibrium core to make its measured ICRR curve linear again. This paper proposes a novel methodology to determine an optimal position for such neutron source installation in the PWR core. The methodology is based on the local adjoint flux distributions obtained from the homogeneous critical adjoint transport equations, which actually represent the importance of the fission neutron source position. The study confirms that the optimal source position is the one with very high homogeneous adjoint fluxes and detector responses, which interestingly is the designed secondary neutron source position in a typical OPR1000 core, as it yields an ICRR curve closest to the traditional 1/M line. Nonetheless, depending on the control rod configuration and the effective source-detector geometry, the optimal source position can actually be different. The paper also clearly demonstrates that the proposed homogeneous critical adjoint flux-based approach can be used to efficiently determine the optimal source-detector geometry in a modern subcritical PWR core.

Table 7 – Detector responses of the four candidate source positions.

Boron concentration (ppm)	k_{eff}	H733	H729	H728	H726
1,726	0.9118	5.72E-10 (0.0555)	1.68E-09 (0.0361)	2.21E-09 (0.0090)	3.35E-09 (0.0138)
1,580	0.9305	9.25E-10 (0.0476)	2.76E-09 (0.0509)	2.88E-09 (0.0273)	4.34E-09 (0.0166)
1,434	0.9425	2.36E-09 (0.0269)	5.02E-09 (0.0380)	4.78E-09 (0.0247)	6.17E-09 (0.0215)
1,288	0.9577	1.18E-08 (0.4858)	1.91E-08 (0.2055)	1.29E-08 (0.1333)	9.56E-09 (0.1242)

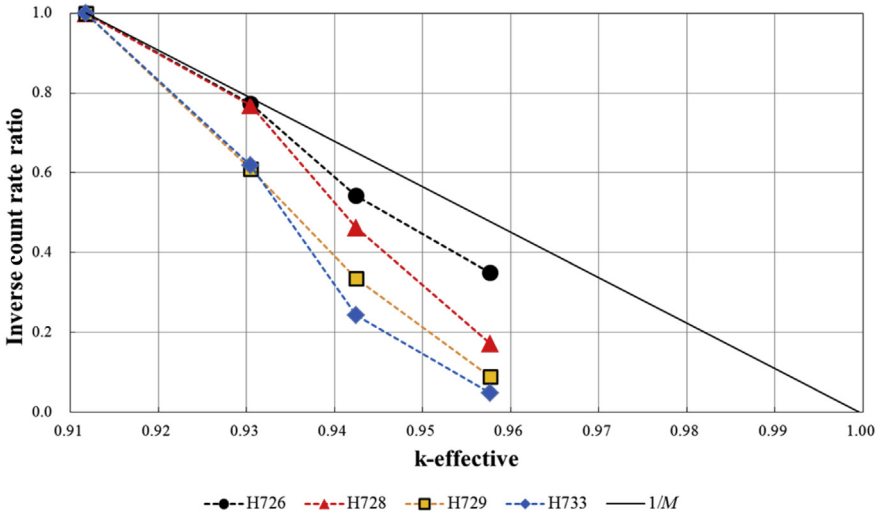

Fig. 10 – Inverse count rate ratio curves of the four candidate source positions at different boron concentrations.

Table 8 – Inverse count rate ratio values at four candidate source positions in the simulated boron dilution accident.

Boron concentration (ppm)	k_{eff}	H733	H729	H728	H726
1,726	0.9118	1.0000	1.0000	1.0000	1.0000
1,580	0.9305	0.6187	0.6090	0.7689	0.7723
1,434	0.9425	0.2424	0.3352	0.4628	0.5425
1,288	0.9577	0.0484	0.0882	0.1719	0.3502

Conflicts of interest

All authors have no conflicts of interest to declare.

Acknowledgments

This work was supported by the Khalifa University of Science, Technology and Research, Korea Advanced Institute of Science and Technology Institute, Daejeon, Korea.

REFERENCES

[1] Nuclear Power Generation Department, Safety Evaluation for a Startup Operation without Neutron Source of Kori Unit 1, Korea Electric Power Company, LTD, 1998.
[2] J.S. Chung, I.T. Woo, The Nuclear Design Report for Ulchin Nuclear Power Plant Unit 3 Cycle 7, Korea Nuclear Fuel Company, 2005. KNF-U3C7–05026 Rev.0.
[3] W. Bojduj, Source Range Detector Response during Boron Dilution Accident at Shutdown, American Nuclear Society: 2010 Annual Meeting, San Diego (CA), 2010, pp. 517–518.
[4] Y.A. Chao, H.Q. Lam, J.D. Gibbons, M.D. Heibel, M. Kauchi, The Spatially Corrected Inverse Count Rate (SCICR) Method for Subcritical Reactivity Measurement, American Nuclear Society: 2004 Annual Meeting, Washington, D.C., 2004, pp. 728–730.
[5] C.A. Ford, Modeling a Source Range Channel Response during a PWR Core Onload Sequence, American Nuclear Society: 2010 Annual Meeting, San Diego (CA), 2010, pp. 639–641.
[6] United States Nuclear Regulatory Commission, Information Notice No. 93–32: Non-conservative Inputs for Boron Dilution Event Analysis, IN-93-32, 1993.
[7] United States Nuclear Regulatory Commission, Generic Letter No. 85–05: Inadvertent Boron Dilution Events, GL-85-05, 1985.
[8] S. Goluoglu, L.M. Petrie Jr., M.E. Dunn, D.F. Hollenbach, B.T. Rearden, Monte Carlo criticality methods and analysis capabilities in SCALE, Nucl. Technol. 174 (2010) 214–235.
[9] S.M. Bowman, SCALE 6: comprehensive nuclear safety analysis code system, Nucl. Technol. 174 (2010) 126–148.
[10] D.E. Peplow, Monte Carlo shielding analysis capabilities with MAVRIC, Nucl. Technol. 174 (2010) 289–313.
[11] H. Nifenecker, S. David, J.M. Loiseaux, O. Meplan, Basics of accelerator driven subcritical reactors, Nucl. Instr. Meth. Phys. Res. A 463 (2001) 428–467.
[12] P. Seltborg, Source efficiency and high-energy neutronics in accelerator-driven systems, Ph.D. Thesis, Department of Nuclear and Reactor Physics Royal Institute of Technology Stockholm, Sweden, 2005.
[13] G.I. Bell, S. Glasstone, Nuclear Reactor Theory, Van Nostrand Reinhold Company, New York, 1970.
[14] K.O. Ott, R.J. Neuhold, Nuclear Reactor Dynamics, American Nuclear Society, Le Grange Park (IL), 1985.
[15] Y. Kim, W.S. Park, C.K. Park, Characterization of a source importance function in an accelerator-driven system, Nucl. Sci. Eng. 144 (2003) 227–241.
[16] J.G. Ahn, N.Z. Cho, J.E. Kuh, Generation of spatial weighting functions for ex-core detectors by adjoint transport calculation, Nucl. Technol. 103 (1993) 114–121.
[17] Scale: A Comprehensive Modeling and Simulation Suite for Nuclear Safety Analysis and Design, 2011. ORNL/TM-2005/39, Version 6.1. Available from Radiation Safety Information Computational Center at Oak Ridge National Laboratory as CCC-785.
[18] S.M. Bowman, O.W. Hermann, M.C. Brady, SCALE-4 Analysis of Pressurized Water Reactor Critical, Oak Ridge National Laboratory, Oak Ridge (TN), ORNL/TM-12294/V2, 1995.